THE JOURNAL OF PHYSICAL CHEMISTRY B

Article

Cite This: J. Phys. Chem. B 2019, 123, 1847−1854

pubs.acs.org/JPCB

Vibrational Cooling in Oligomeric Viologens of Different Sizes and Topologies

Mengdi Liu,[†] Takehiro Kawauchi,[‡] Tomokazu Iyoda,[§] and Piotr Piotrowiak*[,†]

[†]Department of Chemistry, Rutgers University—Newark, 73 Warren Street, Newark, New Jersey 07102, United States

[‡]Department of Materials Chemistry, Faculty of Science and Technology, Ryukoku University, 1-5 Yokotani, Oe-cho, Seta, Otsu, Shiga 520-2194, Japan

[§]Harris Science Research Institute, Doshisha University, 1-3 Tatara Miyakodani, Kyotanabe, Kyoto 610-0394, Japan

Supporting Information

ABSTRACT: Vibrational cooling was investigated in a set of homologous dimers and trimers with methyl viologen repeat units (MV^{2+}). The rapid, <500 fs decay of the D_1 excited state of monoreduced viologen ($MV^{+\bullet}$) via a conical intersection allows the preparation of a vibrationally hot D_0 ground state with a large excess energy of 1.7 eV, which is equivalent to the initial effective temperature of ∼800 K. Pump-probe spectroscopy was used to monitor the disappearance of the characteristic $D_0 \rightarrow D_1$ hot absorption band, which appears at longer wavelengths than the steady-state spectrum of "cold" $MV^{+\bullet}$ in equilibrium with the solvent. It is assumed that the vibrational excitation of the ground is initially confined to the same monoreduced viologen repeat unit, which was optically excited to the localized electronic D_1 state, although some degree of redistribution may occur already in the excited state. The observed cooling rates depend on the size and topology of the oligomer, with the linear trimer exhibiting significantly faster thermalization than the branched one. The experimental results were corroborated by molecular dynamics simulations carried out in the harmonic approximation. The dynamics of the thermal equilibration in these systems appears to be consistent with primarily ballistic initial propagation of the vibrational excess energy over distances as large as ∼4 nm and suggests the presence of interference between the equivalent pathways in the branched trimer.

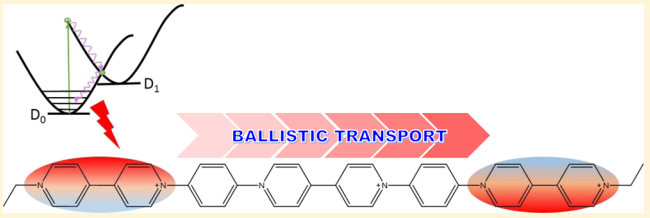

INTRODUCTION

Intramolecular vibrational relaxation (IVR) is a crucial step in the cooling process of optically excited molecules and has been extensively studied both experimentally and theoretically in diverse systems.[1−5] IVR involves the redistribution of excess energy over the vibrational manifold of a certain electronic state. Its time scale can span the range from femtoseconds to a few picoseconds.[6] The IVR process is then followed by vibrational cooling by the environment, which usually takes tens of picoseconds. IVR and subsequent thermal equilibration with the medium are often related to heat conduction because the initial high frequency vibrational excitation is broken down into smaller quanta and ultimately a continuum of classical vibrational and translational motions.[7] From the mechanistic point of view, the transport process can be either ballistic or diffusive, although in most systems, both channels are likely to coexist to some degree.[8,9] Ballistic transport occurs via point-to-point propagation of energy and requires delocalization of the vibrational states over the entire transport distance. It is more pronounced in ordered systems with identical repeat units (crystals, polymers, DNA, and so forth.). Diffusive transport occurs via a Markovian multistep process with random hopping of excitation among the available sites. It is often observed in disordered materials such as glasses or peptides.[7,8,10,11] For molecules in the 5−50 Å size range, the distinction between diffusive and ballistic dynamics is not well defined. In systems whose size is larger than the delocalization length or mean free path of the vibrational excitation, the propagation of energy is dominated by anharmonic interactions. In small molecules, especially at low temperatures, the harmonic behavior is prevalent and the heat flow exhibits a ballistic type of features.[7,12] Numerous experimental and theoretical studies have been carried out to study the IVR and heat transport in a broad variety of systems such as large chromophores connected by bridges,[13,14] alkane chains,[10,11] biomolecules,[15] nanostructures,[9,16] and SAMSs.[17]

Our interest in vibrational relaxation and cooling has been prompted by the pivotal role they play in intramolecular electron-transfer processes occurring on subpicosecond and short picosecond timescales.[18] Because such systems are not fully thermally equilibrated, neither internally nor with the surroundings, they cannot be expected to obey the predictions of the convenient and widely used closed-form theoretical models such as the Marcus or Marcus−Jortner equations, which are based on equilibrium thermodynamics. It has been demonstrated both in molecular systems and at interfaces that

Received: December 18, 2018
Revised: January 23, 2019
Published: February 6, 2019

DOI: 10.1021/acs.jpcb.8b12165
J. Phys. Chem. B 2019, 123, 1847−1854

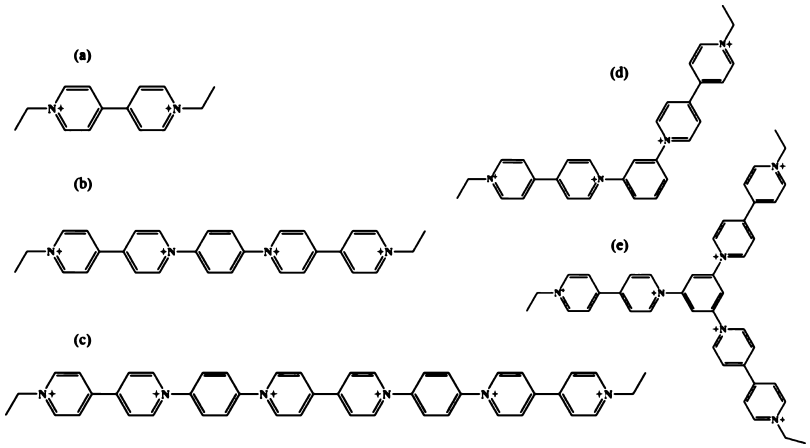

Figure 1. Topology of the oligoviologens: (a) monomer; (b) linear para dimer; (c) linear para trimer; (d) meta dimer; (e) star meta trimer.

electron transfer from vibrationally hot states may be orders of magnitude faster than the equilibrium parameters, leading to unexpected results and interesting venues for the design of light-harvesting materials.[19]

In this paper, we report the investigation of vibrational cooling in a series of oligoviologen arrays shown in Figure 1. Methyl viologen is commonly used in photochemistry, where due to its outstanding ability to accept electrons, it often serves as a building block of the donor−acceptor systems.[20] Upon accepting an electron, the methyl viologen cation becomes the eponymous brightly colored monoreduced radical $MV^{+\bullet}$. Most relevant to this study is the ultrafast internal conversion of the D_1 excited state of $MV^{+\bullet}$ which, within less than 0.5 ps, decays via a conical intersection to the highly vibrationally excited (~1.7 eV) ground state. The formation of the latter has been detected via femtosecond resonance Raman spectroscopy (Huang and Hopkins) and subsequently by transient absorption spectroscopy (Häupl et al.).[21,22] It is therefore an ideal system that allows one to employ electronic excitation to set up nearly instantaneously a localized vibrationally hot state and monitor its subsequent evolution. By altering the number of viologen units and the linkage to the bridge (para and meta), the influence of the molecular size and linear versus branched topology on the energy redistribution and equilibration with the solvent were probed in detail. In the context of this work, it is important to keep in mind that while the evolution and disappearance of the hot ground-state spectrum monotonically follows the vibrational relaxation and thermal equilibration with the solvent, it is generally not a linear reporter of the local temperature but a rather complex product of the Franck−Condon factors weighted by the evolving vibrational populations, with some modes making a greater contribution to the observed response than others. In the case of $MV^{+\bullet}$, the position and the intensity of the ground-state spectrum is sensitive to the distance and dihedral angle between the pyridinium rings. The D_0 ground state has a quinonoid planar structure while the fully relaxed D_1 state approaches a 90° twist. As a result, both the skeletal (high frequency) and torsional (low frequency) normal modes and the corresponding D_0−D_1 Franck−Condon factors have strong influence on the observed decay dynamics and spectral evolution. The low frequency inter-ring twisting mode remains populated at a low residual excess energy and accentuates the slowest component of the thermal equilibration dynamics to a greater degree than it might be seen in a more rigid molecule, in which the excited and ground state geometries are much more similar to one another, for example, the well-studied azulene.[23]

EXPERIMENTAL SECTION

Sample Preparation. Each compound (monomer, linear dimer, linear-trimer, meta dimer, and star trimer) was dissolved in degassed acetonitrile (>99.9%, Sigma-Aldrich) to make a concentrated solution of ~3×10^{-3} M. Excess of zinc powder was added and allowed to react for overnight to singly reduce every viologen unit in each array. Each concentrated solution was diluted using degassed acetonitrile to reach a concentration of ~8×10^{-5} M and pipetted into a 1 cm quartz cell with an air-tight seal for subsequent measurements. All steps were performed in a glove box.

Ground-State Absorption. Absorption spectra of the monomer, linear dimer, and star trimer were measured using a Cary 5000 spectrometer. The absorption spectra of the meta dimer and linear trimer was measured using a Cary 500 spectrometer.

Pump-Probe Spectroscopy. A pulsed laser beam (70 fs, 795 nm) was produced by a mode-locked Ti-sapphire oscillator (Spectra-Physics Tsunami) and amplified by a home-built 1.25 kHz multipass amplifier. The output of the amplifier was split into two streams of pulses. One was converted to white-light continuum in a 2 mm sapphire plate and used as the tunable probe. The other stream was used to drive a noncollinear optical parametric amplifier (Topas White, Light Conversion) and used as the pump beam (550 and 730 nm, 100 μW). The pump pulses were delayed with respect to the probe by a computer-controlled translation stage. The pump and probe beams were spatially overlapped within the sample. The pump was modulated with a mechanical chopper at 50 Hz, and the resulting signal was recorded by a computer-controlled digital lock-in amplifier (Stanford Research, SR810) with a monochromator (Oriel MS257) scanning the desired probe wavelength. Eight scans were averaged in order to achieve a satisfactory signal-to-noise ratio. In the case of the meta dimer, a new laser system was used. In this case 177 fs, 1030 nm-pulsed output was generated by an integrated laser system (PHAROS, Light Conversion). The fundamental output at 2 kHz was split into two trains, one of which was used to pump a noncollinear optical parametric amplifier (ORPHEUS-N 3H) to deliver a pump beam at 550 nm, which was modulated with a mechanical chopper at 50 Hz. The other

DOI: 10.1021/acs.jpcb.8b12165
J. Phys. Chem. B 2019, 123, 1847−1854

pulse train was directed into an ultrafast spectroscopic system (HARPIA-TA) to generate white light continuum as the probe beam, which was spatially overlapped with the pump pulse at the sample. A photodiode array was used to detect the signal.

MO Calculations and Molecular Dynamics Simulations. All molecules were optimized at the B3LYP 6-31G* level using Spartan '16 by Wavefunction, Inc. Classic molecular dynamics (MD) simulations were carried out using the YASARA package with Amber 14 force field in a cubic box with periodic boundary conditions in vacuum. The thermal excitation was simulated by selectively rescaling the atom velocities of the hot viologen unit to reach the initial temperature of 1000 K while the rest of the oligomer remained at 298 K. A time step of 2 × 0.5 fs was used in all simulations and the kinetic energy of all parts of a molecule, including the hot viologens, bridging units, and cold viologens was monitored and plotted versus time. For each structure, five trajectories were collected.

RESULTS AND DISCUSSION

The D_0−D_1 ground state absorption spectra of all four reduced oligomers exhibit a vibronic structure and peak position at 600 nm, which are nearly identical to those of the monomeric $MV^{+\bullet}$ (Figure 2). The trimers show slightly more pronounced broadening of the high energy side of the spectrum, which in the case of the linear para-bridged compound, is magnified by the contributions of the inequivalent sites at the termini and in the center of the molecule. Overall, these differences are minor and do not merit further discussion. By correlating concentration and the measured absorption coefficient, it was concluded that every viologen unit in each oligomer was singly reduced. The close similarity of the spectra shows that the $MV^{+\bullet}$ moieties interact only weakly with one another and that the electronic states of interest remain well localized on just one repeat unit. As a result, in the pump-probe experiments, the excited state and the resulting vibrationally hot ground state are initially localized at a single $MV^{+\bullet}$ site. Because of the low photon density employed in these experiments, the probability of exciting more than one reduced viologen unit per oligomer is negligibly small. The localization of electronic states is supported by the calculated electronic coupling between the lowest unoccupied molecular orbital orbitals of the MV^{2+} sites, which is 68 cm^{-1} for the para and 97 cm^{-1} for the meta linkage. (HF, 6-311+G**, Spartan'16 by Wavefunction, Inc.). The larger interaction in the meta-bridged systems indicates the dominance of the σ coupling pathway.

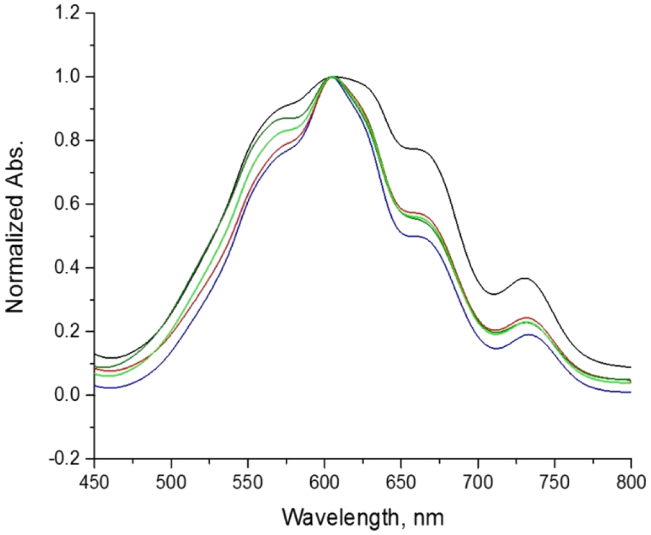

Figure 2. Ground-state absorption of reduced monomer (blue), linear dimer (red), meta dimer (light green), linear trimer (black), and star trimer (olive).

Pump-Probe Experiments. The transient absorption spectra of the four compounds are also similar to one another and display three discernible bands at ∼710, ∼770 and, ∼850 nm (Figure 3), which aside from the red shift, mimic the appearance of the cw spectrum $MV^{+\bullet}$. This similarity and the spectral dynamics lead Häupl et al. to assign the transient spectrum to the vibrationally "hot" electronic ground state rather than the D_1 excited state.[22] The temporal evolution of the transient spectrum reflects the vibrational temperature of the molecule, with the red-most wavelengths reporting the hottest ground state species immediately after the internal conversion and the shorter ones encompassing a broader range of excess energy and persisting at more advanced stages of thermal equilibration with the solvent. Accordingly, the measurements were carried out at three values of λ_{probe}: 845, 762, and 703 nm. On the other hand, similarly to monomeric viologen, the cooling dynamics in the oligomers is only weakly dependent on the excitation wavelength and all results discussed below were obtained at a fixed λ_{exc} = 550 nm. In the $MV^{+\bullet}$ oligomers, the evolving hot spectrum is a sum of contributions from the photoexcited moiety, whose internal temperature decreases throughout the scan, as well as the remaining sites, whose vibrational temperature initially increases until the entire system begins to cool down and equilibrate with the solvent.

The probe wavelength−internal temperature correlation is reflected both in the rise time and the decay of the hot spectrum. As expected, we observed the fastest, ∼240 fs formation of the ground state, at the longest probe wavelength of 845 nm (Table 1). At shorter probe wavelengths, the apparent rate of formation of the hot ground state is slower because the overall rise of the signal is a composite result of direct population by internal conversion combined with vibrational energy redistribution (IVR) from the highest vibrational states. These results are consistent with our prior observations in monomeric $MV^{+\bullet}$, confirming that the electronic interactions between the reduced sites are weak and do not significantly alter the internal conversion process. As in the case of the monomer, the formation rates reported here are faster than the early literature value,[21,22] most likely because of the superior time resolution of the present experimental setup.

The cooling profiles are collected in Figure 4. It is apparent that for all molecules the decay dynamics is by far fastest at the longest probe wavelength of 845 nm, which is sensitive to the hottest population of the ground state. Furthermore, at all probe wavelengths, the cooling process is perceptibly faster in the oligomers than in monomeric viologen; however, the differences among the oligomers are much more subtle. The lack of pronounced dependence on the number of repeat units is consistent with ballistic propagation dominating rather than stochastic, heat-like energy redistribution and intramolecular equilibration.[5,7]

Parameters recovered from double exponential fitting of the decay profiles are gathered in Table 2. In order to achieve convergence, the fitting required the inclusion of a small

DOI: 10.1021/acs.jpcb.8b12165
J. Phys. Chem. B 2019, 123, 1847−1854

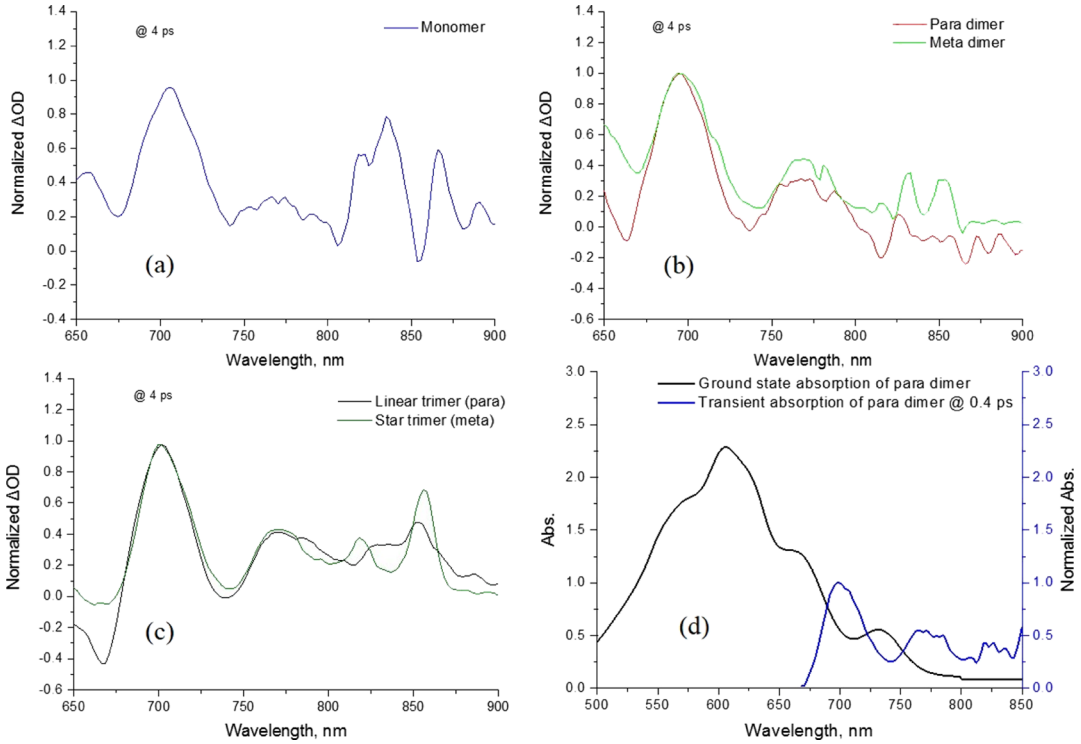

Figure 3. Normalized transient absorption spectra of the reduced (a) monomer (blue); (b) linear dimer (red) and meta dimer (light green); (c) linear trimer (black) and star trimer (olive) at 4 ps after excitation at 550 nm. (d) Overlay of ground-state absorption and the TA spectrum of the reduced linear dimer at 4 ps after excitation.

Table 1. Rise Time of Different Probed Populations in the Linear Dimer Excited at 550 nm

λ_{probe}, nm	703	762	845
rise time, fs	562 ± 22	317 ± 13	239 ± 17

adjustable offset, A_∞, of variable magnitude. The origin of this behavior is uncertain and we tentatively ascribe it to residual thermal lensing. Given the complexity of the cooling process, empirical fitting parameters do not have a direct mechanistic correspondence, however, the existence of two general regimes can be identified. The initial, steep decay of the hot population occurs with τ_1 = 1.4−2.3 ps, while the slow component τ_2 extends all the way to 18 ps, consistent with IVR dominating the early times followed by slower dissipation to the solvent. Indeed, the above range of τ_1 values agrees remarkably well with the ∼2 ps time constant reported by Huang et al. for the cooling of the in-plane C−C skeletal modes in monomeric $MV^{+\bullet}$, as measured in their time-resolved resonance Raman experiments. The biphasic nature of the equilibration is most pronounced at the longer wavelengths, where the fast/slow ratio is as high as ∼5. At short wavelengths, this ratio drops to approximately 2 and the monomer trace at 703 nm can be fitted only with a single exponential. This behavior is reasonable because, as mentioned earlier, the longest wavelengths report the vibrationally hottest ground state, while the short ones are biased toward the already internally equilibrated molecules, where stochastic heat transfer to the solvent should dominate the response. It should be noted that the ionic nature of viologens restricts the choice of solvents to the strongly polar ones and limits the ability to more decisively separate the intramolecular and solvent-controlled regimes of the cooling process.

The substantial crosstalk between the fitting parameters in Table 2 (both the time constants and the corresponding amplitudes of the fast and slow decay components) cautions one not to overinterpret the differences between individual rates and amplitudes. With the τ_1/τ_2 ratio rarely exceeding 3, the time constants are not very well separated, and it is helpful to examine the data plotted as survival time τ_s of a certain fraction of the initial population (Figure 5). In this simplistic representation, at the longest probe wavelengths reporting initial stages of the equilibration, the behavior of all four oligomers is practically indistinguishable, reinforcing the notion that ballistic propagation of vibrational energy dominates the early stages of the cooling process. The greatest differences among the examined systems are seen at the shortest probe wavelength, λ_{probe} = 703 nm, that is, for the already internally equilibrated and somewhat cooled molecules. While the dimers are nearly indistinguishable from one another or the monomer, the trimers reach thermal equilibrium with the solvent up to 35% sooner. This difference is likely a combined outcome of the increased surface area of the trimers, which is partially balanced by a lower temperature gradient between the molecule and the solvent upon the completion of intramolecular redistribution of the vibrational energy among three rather than two viologen moieties. Very interestingly, at 703 nm, the cooling profiles of the linear and star trimer diverge, with the latter exhibiting ∼15% slower relaxation. This divergence cannot be rationalized in terms of simple surface area or number of vibrational modes arguments and suggests the possibility of vibrational interference between the equivalent pathways in the branched meta-bridged system.

MD Simulations. Standard pump-probe spectra and decay profiles monitor only the average evolution of the ensemble and cannot unravel the full complexity of the intramolecular

DOI: 10.1021/acs.jpcb.8b12165
J. Phys. Chem. B 2019, 123, 1847−1854

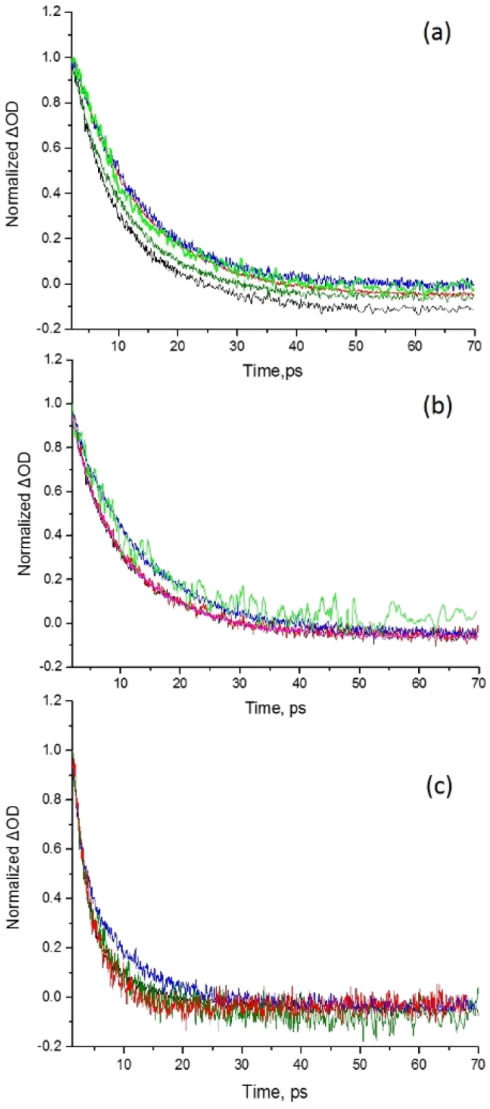

Figure 4. Transient absorption decay profiles for the monomer (blue), linear dimer (red), *meta*-dimer (light green), linear trimer (black), and star trimer (olive) excited at 550 nm and probed at different wavelengths: (a) 703; (b) 762; and (c) 845 nm.

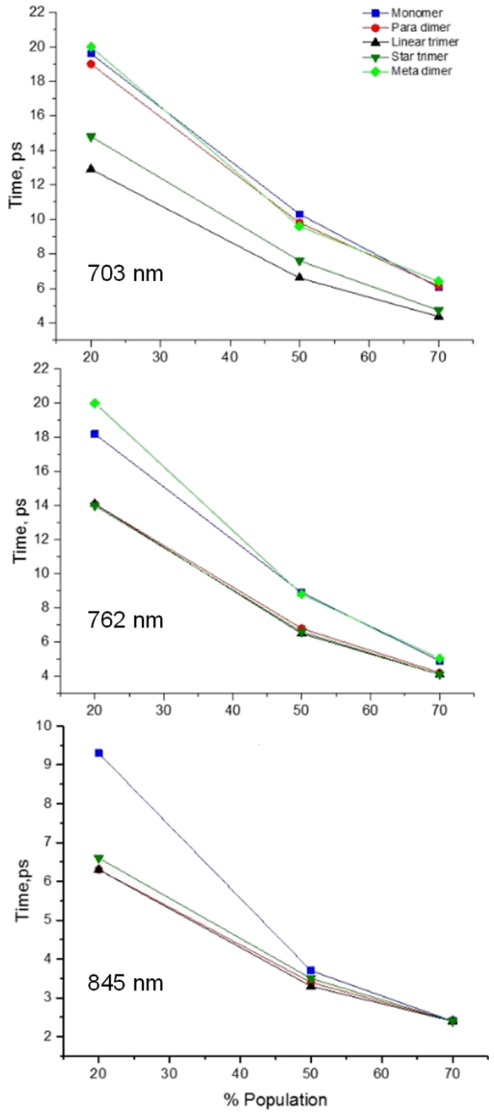

Figure 5. Survival time vs population at different probe wavelengths for the monomer (blue); linear dimer (red); meta dimer (light green); linear trimer (black); star trimer (green).

Table 2. Double Exponential Decay Fitting Parameters of Five Compounds Excited at 550 nm and Probed at Different Wavelengths

λ_{probe}		τ_1/ps	A_1	τ_2/ps	A_2	A_∞
703 nm	monomer	11 ± 0.04	0.89 ± 0.002			0.1 ± 0.0005
	linear dimer	8.3 ± 0.6	0.49 ± 0.1	15 ± 1	0.57 ± 0.1	−0.06 ± 0.001
	meta dimer	9 ± 1.5	0.71 ± 0.3	18 ± 5	0.34 ± 0.26	−0.04 ± 0.002
	linear trimer	5.0 ± 0.3	0.57 ± 0.05	14 ± 0.8	0.56 ± 0.05	−0.12 ± 0.002
	meta trimer	3.7 ± 0.4	0.16 ± 0.03	11 ± 0.2	0.85 ± 0.03	−0.06 ± 0.001
762 nm	monomer	8.6 ± 0.1	0.49 ± 0.3	15 ± 0.3	0.51 ± 0.03	−0.05 ± 0.003
	linear dimer	3.3 ± 0.3	0.28 ± 0.03	11 ± 0.2	0.77 ± 0.03	−0.05 ± 0.001
	meta dimer	3.5 ± 0.2	0.22 ± 0.07	11 ± 0.5	0.74 ± 0.09	0.01 ± 0.006
	linear trimer	3.9 ± 0.2	0.38 ± 0.03	12 ± 0.3	0.67 ± 0.03	−0.07 ± 0.001
	meta trimer	3.4 ± 0.01	0.25 ± 0.01	11 ± 0.01	0.81 ± 0.001	−0.06 ± 0.001
845 nm	monomer	1.7 ± 0.07	0.44 ± 0.01	9.1 ± 0.2	0.57 ± 0.01	−0.04 ± 0.001
	linear dimer	1.4 ± 0.7	0.17 ± 0.1	3.6 ± 0.2	0.88 ± 0.01	−0.04 ± 0.003
	linear trimer	2.2 ± 0.04	0.75 ± 0.01	10 ± 0.4	0.28 ± 0.01	−0.05 ± 0.001
	meta trimer	2.3 ± 0.2	0.69 ± 0.04	8.8 ± 0.7	0.39 ± 0.05	−0.08 ± 0.002

DOI: 10.1021/acs.jpcb.8b12165
J. Phys. Chem. B 2019, 123, 1847−1854

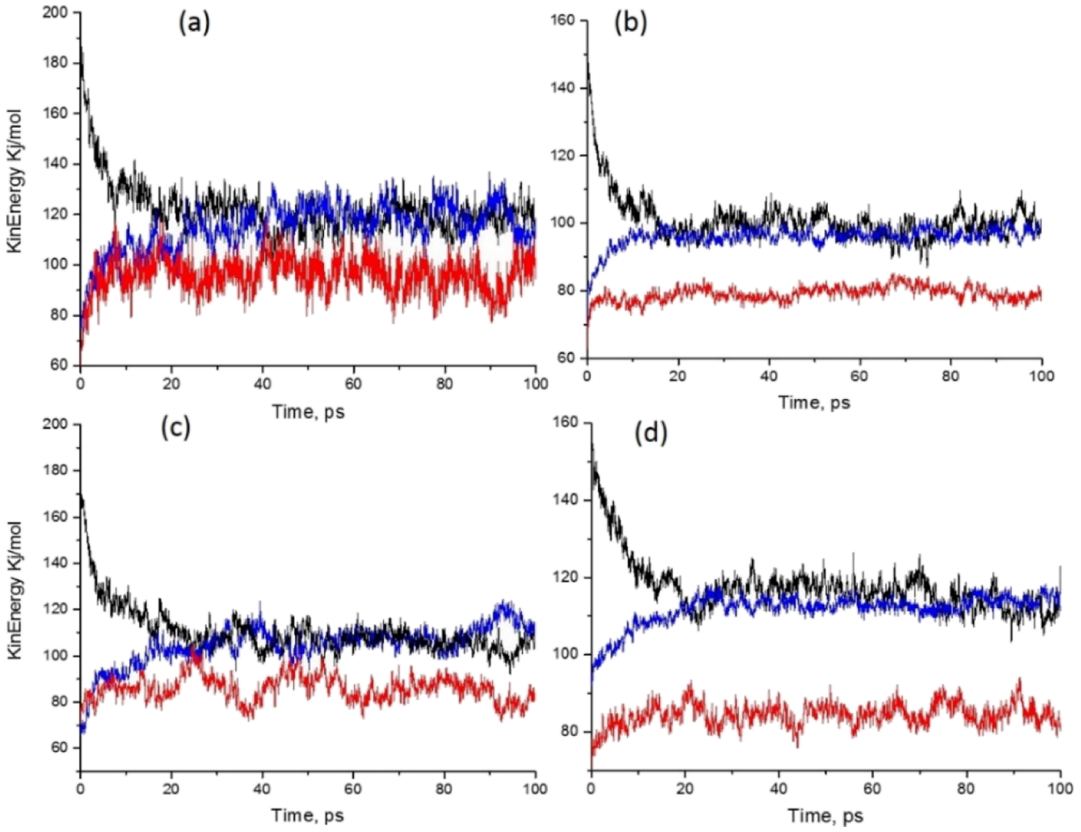

Figure 6. Averaged MD trajectories of the hot viologen (black), cold viologen (blue), and the bridge (red) in: (a) liner dimer; (b) linear trimer; (c) meta dimer; (d) meta "star" trimer.

heat flow and the cooling process. Classical MD simulations in the harmonic approximation were carried out in order to augment our understanding of the underlying vibrational energy redistribution, especially at early times. Among others, the calculations allowed us to selectively deposit excess vibrational energy in the terminal versus central viologen unit of the linear trimer, a feat which is not possible experimentally, given the indistinguishable absorption spectra. Similarly, we could monitor not only the energy loss atthe initially excited site but also the vibrational energy gain of the remaining viologens and bridging units. The computational procedures were selected to realistically mimic the conditions and limitations of the experiment. Because our pump-probe measurements do not reveal any vibrational coherence and, unless a strongly coupled dominant mode is present, are not very sensitive to such effects, it was chosen to "heat" a monomeric viologen moiety to 1000 K at the beginning of the simulation in a random fashion while the rest of the oligomer remained at room temperature. The initial temperature of the hot viologen was estimated on the basis of the known excitation energy (18 200 cm^{-1}) and the number of normal modes. By simulating the vibrational excitation via rescaling of atom velocities rather than depositing an equivalent amount of energy in an individual mode, which may be selectively populated upon passing through the conical intersection, any unintended mode specificity at the outset of the simulation was avoided.

Each trajectory shown in Figure 6 is an average of five individual simulations. The trajectories were analyzed by double exponential fitting in order to allow a more direct comparison with the experiment. In some instances, no stable biexponential fits could be obtained. The loss of energy by the hot viologen and the corresponding gain by the remainder of the molecule is evident in all traces. Given the simplicity of the model, the qualitative agreement with the experimental results, especially at early times after photoexcitation, is good. For example, the biphasic equilibration in the linear dimer (Figure 6a) consists of components with τ_1 = 2.0 ± 0.1 ps and τ_2 = 11.0 ± 0.4 ps. The former time constant agrees very well with the experimental τ_1 = 1.4 ± 0.7 ps, while the latter is considerably slower than the measured value of τ_2 = 3.6 ± 0.4 ps. This is likely to reflect the importance of anharmonicity and heat transfer to the solvent in the experimental system. The trajectories for the star trimer can be fitted only with a single exponential with τ = 5.9 ± 0.1 ps.

In the dimers, we observe very similar time scales for the loss of energy by the hot viologens and energy gain by the cold moieties, again pointing to the ballistic rather than the stochastic nature of the process. In both trimers, there is an indication of a more gradual propagation of the energy across the system, with the vibrational excitation arriving to the bridging units at least twice as fast as to the terminal cold viologens (Table 3). This behavior is more pronounced in the case of the linear trimer. The stepwise transfer of vibrational energy is consistent with a stochastic, heatlike transport, which appears to gain importance; as the size of the oligomer increases, the ballistic propagation becomes less dominant.

Lastly, it is of interest to compare the behavior of the para- (linear) versus meta-bridged trimers. The linear dimer and trimer show qualitatively similar temporal profiles, with, as expected, the trimer equilibrating faster. Their meta-bridged trimer appears to lack the well-defined ~1 ps fast component,

DOI: 10.1021/acs.jpcb.8b12165
J. Phys. Chem. B 2019, 123, 1847−1854

Table 3. Time Constants and Normalized Amplitudes Obtained from Fitting of the MD Vibrational Equilibration Trajectories[a]

	τ_1/ps	A_1	τ_2/ps	A_2
Energy Loss by the Hot Viologen				
linear dimer	2.0 ± 0.08	0.63 ± 0.01	11 ± 0.4	0.37 ± 0.01
meta dimer	1.1 ± 0.05	0.65 ± 0.03	11 ± 0.2	0.35 ± 0.004
linear trimer	0.76 ± 0.06	0.40 ± 0.01	5.2 ± 0.09	0.60 ± 0.01
star trimer	5.9 ± 0.05	1.0		
Energy Gain by the Cold Viologens				
linear dimer	1.1 ± 0.08	0.5 ± 0.03	23 ± 0.4	0.5 ± 0.006
meta dimer	0.99 ± 0.06	0.54 ± 0.03	12 ± 0.2	0.46 ± 0.005
linear trimer	3.8 ± 0.04	1.0		
star trimer	8.4 ± 0.06	1.0		
Energy Gain by the Bridging Moieties				
linear dimer	1.6 ± 0.05	1.0		
meta dimer	2.2 ± 0.05	1.0		
linear trimer	0.57 ± 0.03	1.0		
star trimer	4.0 ± 0.1	1.0		

[a]In the case of missing entries, no stable fit was possible.

which in all other compounds accounts for 40−65% of the relaxation. Similarly, as in the case of the experimental results, the equilibration in the star trimer is slower than in the linear analogue, suggesting that the redistribution of energy in the branched topology is hampered by the symmetry and vibrational interference between the equivalent pathways. The difference in the dynamics of the linear versus star trimer topology is more pronounced in the simulation traces (Figure 6b,d, Table 3), most likely because of the simple harmonic model, which unrealistically accentuates coherence effects. It should be noted that conceptually similar interference effects were predicted theoretically for electron transfer in symmetric branched systems consisting of a single donor and multiple acceptors.[24]

CONCLUSIONS

The redistribution of excess energy undergoes acceleration upon the addition of viologen units to the monomer and points to a major ballistic component of the process which allows a substantial fraction of the vibrational energy spread over the length of nearly 4 nm in just a few picoseconds. Perhaps most interestingly, equilibration in the branched star trimer is considerably slower than in its linear counterpart. The dependence on the branching topology suggests that the skeletal modes propagate ballistically along the oligomer backbone. Branching in the star trimer leads to mode degeneracies and imposes symmetry barriers on the ballistic propagation. MD simulations carried out within the harmonic approximation corroborate the importance of ballistic effects and the influence of topology on the propagation of vibrational excess energy in these systems. These findings have fascinating implications for electron-transfer processes in donor−acceptor systems in which one or both partners are far from thermal equilibrium, for example, in the dendritic networks of electron acceptors, which were recently studied by this group.[18] Depending on the details of the electronic coupling and the driving force, ballistic propagation of vibrational excitation may allow the heat front to propagate along the oligomeric system considerably faster than the tunneling or hopping electron, thus dynamically altering the effective local temperature and the driving force landscape for the subsequent electron transfer events. In a system containing multiple closely spaced acceptor sites, such situation is likely to occur spontaneously, whenever the initial photoinduced charge separation process occurs at a large driving force.

ASSOCIATED CONTENT

Supporting Information

The Supporting Information is available free of charge on the ACS Publications website at DOI: 10.1021/acs.jpcb.8b12165.

Transient absorption spectra for the monomer, linear dimer, linear trimer, and star trimer recorded at different delay times after photoexcitation at 550 nm (PDF)

AUTHOR INFORMATION

Corresponding Author

*E-mail: piotr@newark.rutgers.edu.

ORCID

Takehiro Kawauchi: 0000-0001-5394-8178

Piotr Piotrowiak: 0000-0003-0134-3227

Notes

The authors declare no competing financial interest.

ACKNOWLEDGMENTS

The authors would like to thank the NSF-JSPS International Collaboration in Chemistry Program for partial support of this project through the NSF grant 1415881. The instrumentation used in the course of this research acquired with the help of US DOE Office of Basic Energy Research grant DE-FG-06ER15828 and NSF MRI grants 0923345 and 1726345 to P.P. T.K. acknowledges generous support by the JSPS KAKENHI grant no. 15K04590. P.P. wishes to acknowledge helpful discussion with Drs. Michael Wasielewski and Leif Hammarstrom.

REFERENCES

(1) Felker, P. M.; Zewail, A. H. Dynamics of Intramolecular Vibrational-Energy Redistribution (IVR). II. Excess Energy Dependence. *J. Chem. Phys.* **1985**, *82*, 2975−2993.

(2) Felker, P. M.; Zewail, A. H. Dynamics of Intramolecular Vibrational-Energy Redistribution (IVR). I. Coherence Effects. *J. Chem. Phys.* **1985**, *82*, 2961−2974.

(3) Nesbitt, D. J.; Field, R. W. Vibrational Energy Flow in Highly Excited Molecules: Role of Intramolecular Vibrational Redistribution. *J. Phys. Chem.* **1996**, *100*, 12735−12756.

(4) Uzer, T.; Miller, W. H. Theories of Intramolecular Vibrational Energy Transfer. *Phys. Rep.* **1991**, *199*, 73−146.

(5) Schwarzer, D.; Kutne, P.; Schröder, C.; Troe, J. Intramolecular Vibrational Energy Redistribution in Bridged Azulene-Anthracene Compounds: Ballistic Energy Transport Through Molecular Chains. *J. Chem. Phys.* **2004**, *121*, 1754−1764.

(6) Sukowski, U.; Seilmeier, A.; Elsaesser, T.; Fischer, S. F. Picosecond Energy Transfer of Vibrationally Hot Molecules in Solution: Experimental Studies and Theoretical Analysis. *J. Chem. Phys.* **1990**, *93*, 4094−4101.

(7) Segal, D.; Agarwalla, B. K. Vibrational Heat Transport in Molecular Junctions. *Annu. Rev. Phys. Chem.* **2016**, *67*, 185−209.

DOI: 10.1021/acs.jpcb.8b12165
J. Phys. Chem. B 2019, 123, 1847−1854

(8) Chen, G. Ballistic-Diffusive Equations for Transient Heat Conduction From Nano to Macroscales. *J. Heat Transfer* **2002**, *124*, 320.
(9) Shiomi, J.; Maruyama, S. Molecular Dynamics of Diffusive-Ballistic Heat Conduction in Single-Walled Carbon Nanotubes. *Jpn. J. Appl. Phys.* **2008**, *47*, 2005−2009.
(10) Kurnosov, A. A.; Rubtsov, I. V.; Burin, A. L. Communication: Fast Transport and Relaxation of Vibrational Energy in Polymer Chains. *J. Chem. Phys.* **2015**, *142*, 011101.
(11) Rubtsova, N. I.; Nyby, C. M.; Zhang, H.; Zhang, B.; Zhou, X.; Jayawickramarajah, J.; Burin, A. L.; Rubtsov, I. V. Room-Temperature Ballistic Energy Transport in Molecules with Repeating Units. *J. Chem. Phys.* **2015**, *142*, 212412.
(12) Segal, D.; Nitzan, A.; Hänggi, P. Thermal Conductance Through Molecular Wires. *J. Chem. Phys.* **2003**, *119*, 6840−6855.
(13) Wild, W.; Seilmeier, A.; Gottfried, N. H.; Kaiser, W. Ultrafast Investigations of Vibrationally Hot Molecules After Internal Conversion in Solution. *Chem. Phys. Lett.* **1985**, *119*, 259−263.
(14) Wurzer, A. J.; Wilhelm, T.; Piel, J.; Riedle, E. Comprehensive Measurement of the S_1 Azulene Relaxation Dynamics and Observation of Vibrational Wavepacket Motion. *Chem. Phys. Lett.* **1999**, *299*, 296−302.
(15) Pecourt, J.-M. L.; Peon, J.; Kohler, B. DNA Excited-State Dynamics: Ultrafast Internal Conversion and Vibrational Cooling in a Series of Nucleosides. *J. Am. Chem. Soc.* **2001**, *123*, 10370−10378.
(16) Cahill, D. G.; Ford, W. K.; Goodson, K. E.; Mahan, G. D.; Majumdar, A.; Maris, H. J.; Merlin, R.; Phillpot, S. R. Nanoscale Thermal Transport. *J. Appl. Phys.* **2003**, *93*, 793−818.
(17) Rubtsova, N. I.; Qasim, L. N.; Kurnosov, A. A.; Burin, A. L.; Rubtsov, I. V. Ballistic Energy Transport in Oligomers. *Acc. Chem. Res.* **2015**, *48*, 2547−2555.
(18) Gong, Z.; Bao, J.; Nagai, K.; Iyoda, T.; Kawauchi, T.; Piotrowiak, P. Generation Dependent Ultrafast Charge Separation and Recombination in a Pyrene-Viologen Family of Dendrons. *J. Phys. Chem. B* **2016**, *120*, 4286−4295.
(19) Myahkostupov, M.; Pagba, C. V.; Gundlach, L.; Piotrowiak, P. Vibrational State Dependence of Interfacial Electron Transfer: Hot Electron Injection from the S_1 State of Azulene into TiO_2 Nanoparticles. *J. Phys. Chem. C* **2013**, *117*, 20485−20493.
(20) Monk, P. M. S. *The Viologens: Physicochemical Properties, Synthesis, and Applications of the Salts of 4,4′-Bipyridine*; Wiley: Chichester, New York, 1998; p xix, p 311.
(21) Huang, Y.; Hopkins, J. B. Femtosecond Resonance Raman Investigation of Four Univalent Bipyridinium Radicals. *J. Phys. Chem.* **1996**, *100*, 9585−9591.
(22) Häupl, T.; Lomoth, R.; Hammarström, L. Femtosecond Dynamics of the Photoexcited Methyl Viologen Radical Cation. *J. Phys. Chem. A* **2003**, *107*, 435−438.
(23) Hochstrasser, R. M.; Nyi, C. A. Resonance fluorescence, Raman Spectra and Relaxation of Single Vibronic Levels in the Condensed Phase: Azulene in Naphthalene. *J. Chem. Phys.* **1979**, *70*, 1112−1128.
(24) Risser, S. M.; Beratan, D. N.; Onuchic, J. N. Electronic Coupling in Starburst Dendrimers: Connectivity, Disorder, and Finite Size Effects in Macromolecular Bethe Lattices. *J. Phys. Chem.* **1993**, *97*, 4523−4527.

DOI: 10.1021/acs.jpcb.8b12165
J. Phys. Chem. B 2019, 123, 1847−1854